Chapter 2
Electromagnetic Transitions as a Probe of Nuclear Clustering

David G. Jenkins

2.1 Introduction

Nuclear clustering was first suggested as an explanation for anomalous structure in the elastic and inelastic scattering of two ^{12}C nuclei. This concept has latterly been extended to encompass all light alpha-conjugate nuclei, where bandheads for highly-deformed rotational structures are expected on or near the threshold energies for break-up into different alpha-cluster channels. Traditionally, such cluster states have often been identified on the basis of the position of resonances seen in fusion [1], (in)elastic scattering [2] and break-up reactions [3, 4]. Such states are then assigned to rotational bands, often with the aid of comparison to theoretical expectations. Clustering in nuclei has therefore often been the province of reaction studies but this approach is not without ambiguity, and runs the risk of over-enthusiastic interpretation of experimental data. The states observed may appear to follow a rotational pattern but it is not an obvious step to say that they share the same intrinsic configuration.

This chapter will stress the very important role that the observation of electromagnetic transitions between candidate cluster states or superdeformed states in light alpha-conjugate nuclei could play in securing the whole basis of the cluster model. Since clustering is generally associated with large intrinsic deformations, very enhanced *E2* transitions are expected between states in cluster bands. Moreover, different cluster configurations with large intrinsic deformations may also be connected by *E0* transitions between states of the same angular momentum. The strength of such transitions is related to the difference in the mean squared charge radius [5].

A second topic explored in this chapter will be the electromagnetic decay of cluster resonances into normal states. A very relevant example of this is heavy-ion

D.G. Jenkins (✉)
Department of Physics, University of York, York YO10 5DD, UK
e-mail: david.jenkins@york.ac.uk

C. Beck (ed.), *Clusters in Nuclei, Volume 3*, Lecture Notes in Physics 875,
DOI 10.1007/978-3-319-01077-9_2,

radiative capture. In all the cases considered here, the experimental challenges are strong and similar in character, and relate to the fact that:

- States with a strong cluster configuration are often particle-unbound and frequently lie at very high excitation energy. Phase space considerations dictate that electromagnetic branches in such cases will be small, and competition from break-up channels will be strong.
- The relevant transition energies are, in general, high (1 MeV and up) and so are challenging to measure with both high resolution and high efficiency.
- Cluster states, although unbound, are often "narrow", typically 100s of keV wide although in many cases this is most probably an instrumental width and not the true width.

2.2 Gamma-Ray Spectroscopy

The principal experimental methodology appropriate to these studies is γ-ray spectroscopy. This technique is discussed in Chap. 6 of Vol. 2 of this series by Papka and Beck, but it is worth reviewing some of the key aspects of such measurements again here, in terms of the relevant detection technology and some of the methods which can be used to extract important information on the states between which gamma decay takes place.

Gamma-ray spectroscopy supplies information on the energy of electromagnetic transitions, and their relative intensity. Analysis of coincidence data allows a level scheme to be constructed. For reactions where magnetic substate alignment is achieved, it is possible to use the angular distribution of gamma rays to extract the multipolarity of the transition. In addition, gamma-ray spectroscopy can be used to deduce transition strengths from lifetimes (corrected for particle-emission in the case of unbound states). In the case of light alpha-conjugate nuclei where typical lifetimes are in the order of femtoseconds, an appropriate technique is the fractional Doppler-shift technique comparing the reduced Doppler shift observed for transitions with a finite lifetime due to slowing in the target.

There are two principal classes of gamma-ray detector which may be used in the study of gamma rays associated with clustering, and both types have been used in the studies to be described here. The first class of detector employ inorganic scintillators. Such detectors have the advantage of a high intrinsic efficiency but at the expense of limited energy resolution. Typical scintillator materials include sodium iodide, barium fluoride, bismuth germinate (BGO) and caesium iodide. Scintillation light is produced by the interaction of gamma rays in the crystal, and is usually collected and amplified using a photomultiplier tube (PMT). The best resolution for scintillator detectors with conventional scintillator materials is around 6–7 % for 662-keV gamma rays obtained for sodium iodide detectors. Novel materials such as lanthanum bromide are now becoming available which can obtain a resolution below 3 %. The future prospects with such novel scintillators will be reviewed briefly at the end of this chapter.

The second type of detector relevant to gamma-ray spectroscopy are germanium detectors, of which the most modern type are hyper-pure germanium detectors. Such detectors are semiconductor-based and have an extremely high intrinsic energy resolution of the order of a few keV. In general, though, the efficiency of such detectors is considerably lower (typically an order of magnitude) than that achievable with a scintillator detector. The principal reason for this reduced efficiency is the general practice of surrounding germanium crystals with a high efficiency scintillator shield to veto Compton-scattered gamma rays. This ensures an excellent peak-to-total but means that only gamma rays which deposit all of their energy in the germanium crystal are accepted. The degradation in efficiency is energy dependent and is significantly worse for high-energy gamma rays. The next generation of germanium detector array, for example AGATA [6], dispenses with the veto shield and comprises a complete germanium shell. Gamma-ray interactions are then studied through tracking. This approach leads to significantly higher efficiency for detecting a single gamma ray, but orders of magnitude greater efficiency for detecting large multiplicities of gamma rays in coincidence. Such next generation arrays are yet to be applied to studies of nuclear clustering but the prospects are exciting.

2.3 Physics Examples

2.3.1 Molecular Transitions in ^{8}Be

An excellent test case for the cluster model is ^{8}Be since the ground state is already suggested to be based on alpha-clustering [7, 8]. The unbound excited states built on this configuration have an energy spacing consistent with strong deformation (see Fig. 2.1). In recent years, increase in computer power has made it possible to perform *ab initio* calculations for light nuclei. In the case of ^{8}Be, they point to a strong α-α cluster configuration for its ground state (see Fig. 2.2) [9]. There are, therefore, competing descriptions of ^{8}Be within very different model prescriptions.

A strong test of the competing models would be to measure the strength of the electromagnetic transitions connecting the states in the ground state band. Langanke and Rolfs have calculated the transition strength for $2^{+} \rightarrow 0^{+}$ [10] and obtain $\Gamma_{\gamma} = 8.3$ meV corresponding to a transition of 75 Wu. In a separate work, they calculated the $4^{+} \rightarrow 2^{+}$ transition strength to be 19 Wu [11]. Despite the fact that the in-band transitions are "strong", the gamma branch is such a small fraction of the total width of the state, that it is extremely challenging to attempt to discriminate it. It turns out that the prospects are much more favourable for measuring the $4^{+} \rightarrow 2^{+}$ transition than the $2^{+} \rightarrow 0^{+}$ transition.

Datar et al. have carried out a "brute-force" determination of the $4^{+} \rightarrow 2^{+}$ transition strength in an experiment at the Tata Institute for Fundamental Research in Mumbai [12]. The measurement comprised a coincidence between a detected gamma ray in an array of BGO detectors with alpha particles from the break-up of

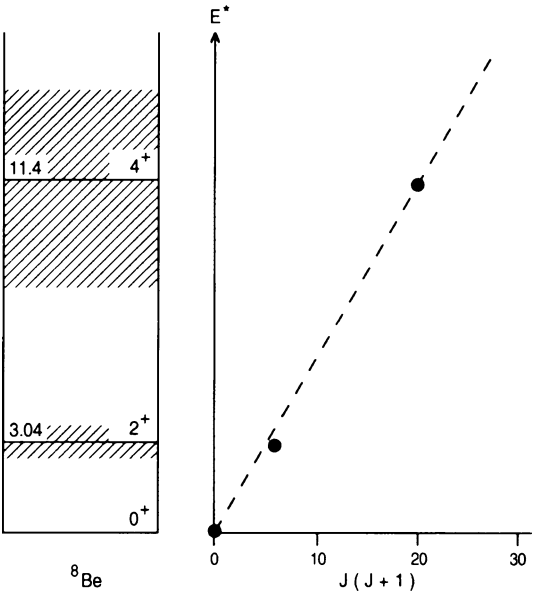

Fig. 2.1 Level diagram for ^{8}Be and excitation energy of states as a function of $J(J+1)$ (taken from [4])

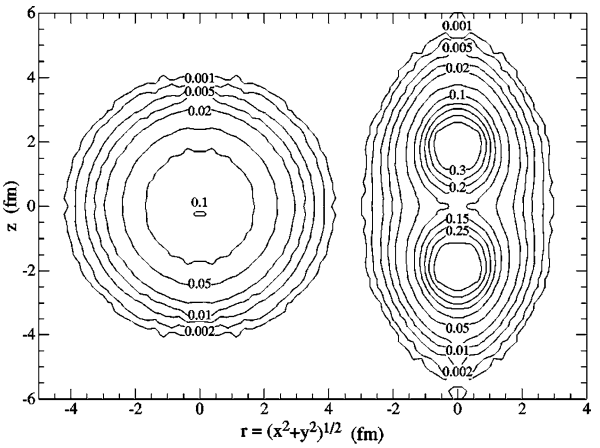

Fig. 2.2 Contours of constant density for ^{8}Be ground state in lab frame (*left*) and intrinsic frame (*right*) taken from Fig. 15 of [9]

the 2^{+} state in ^{8}Be. The B(E2) value obtained is 25(8) e^2 fm^4. This value is consistent with the predictions of both *ab initio* and cluster model calculations. The precision of the measurement, however, does not make it possible to discriminate between these two different models. Accordingly, Datar et al. have repeated their ^{8}Be experiment in 2010 using superior silicon detectors with the aim of reducing the error bar on the B(E2) value in order to discriminate between different theoretical models. This data is under analysis at the time of writing.

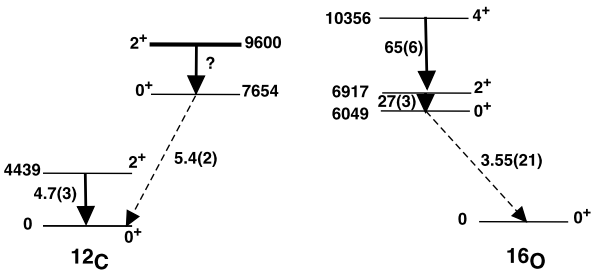

Fig. 2.3 Selected positive parity states in ^{12}C and ^{16}O. B(E2) values are given in Wu where known. The M(E0) transition strengths are given in fm^2

2.3.2 Alpha Clustering in ^{12}C

A long-discussed and spectacular example of a cluster state is the first-excited 0^+ state in ^{12}C. The existence of this state was first hypothesised by Hoyle as a means of explaining the formation of ^{12}C in massive stars [13] and latterly observed by Cook et al. [14] close to the triple-alpha threshold in ^{12}C. The literature on the properties of this state alone is very extensive. The "Hoyle" state clearly has a very complex structure. A shell-model calculation cannot account for its existence but it does appear in various cluster models, and very recently was first described within an *ab initio* model [15]. Recently, Freer et al. [16] reported the possible existence of a 2^+ state at 9.6(1) MeV in ^{12}C with a width of 600(100) keV (see Fig. 2.4). It is argued that this state corresponds to the first member of the rotational band built on the Hoyle state. Locating this state was extremely challenging as it sits underneath an extremely broad 0^+ state at 10.3 MeV. In the context of the present discussion, the observation of an *E2* transition connecting this 2^+ state to the 0^+ "Hoyle" state and measuring its transition strength would be sensational as it would provide extremely important information regarding the nature of the "Hoyle" state. It would, however, be extremely difficult to realise as the gamma width might be expected to be of the order of 10^{-5} of the width of the state. A highly efficient particle-gamma experimental setup would be required. It is also not clear what would be the best choice of reaction to selectively populate the 2^+ state while allowing for γ-ray detection. For completeness, it is worth mentioning that a deformed band is well known in ^{16}O (see Fig. 2.3), and has been described within the cluster model [17].

2.3.3 E0 Transitions

As discussed in the introduction, *E0* transitions are commonly associated with a change in the nuclear radius and may therefore be a relevant observable in terms of nuclear clustering. The width for pair decay of the Hoyle state has recently been extracted from re-analysis of ^{12}C(e,e$'$) data as $\Gamma_\Pi = (62.3 \pm 2.0)$ μeV which is around 10^{-6} of the total width of the state [18]. This corresponds to a monopole strength $M(E0) = 5.4(0.2)$ fm^2 (see Fig. 2.4), and exhausts about 7.5 % of the energy-weighted monopole sum rule. In ^{16}O, the $M(E0)$ value between the ground

state and the first and second excited 0^+ states at $E_{ex} = 6.05$ MeV and 12.05 MeV which are proposed to have $^{12}C+\alpha$ cluster structure are 3.55 ± 0.21 fm^2 and 4.03 ± 0.09 fm^2, respectively, which share about 3 % and 8 % of the energy weighted sum rule value.

At first glance, the large values for the *E0* transitions in these light nuclei are a surprise because the single-particle estimate might be assumed to be a strong overestimate given the very complex structure of the cluster state. Yamada et al. [19] have presented an example calculation for ^{12}C which tries to account for the strong enhancement of the observed *E0* transition. They attribute it to an excitation of the 3α degrees of freedom in the ground state, which then strongly populates the excited "Hoyle" state. These considerations suggest that further experimental investigations of *E0* transitions in alpha-conjugate may pose a strong challenge to theory and be supportive of the complex nature of these states.

2.4 $^{12}C + ^{12}C$ Clustering

The clustering hypothesis was first introduced in the 1960s [20] to explain the anomalous behaviour seen in fusion [1] and elastic and inelastic scattering of two ^{12}C nuclei [2]. Strong resonances were seen below the Coulomb barrier and persisting to the lowest energies considered. The resonances were explained in terms of the formation of short-lived $^{12}C + ^{12}C$ molecules. This system remains the most studied so far as nuclear clustering is concerned and it has strong implications for other related fields such as nuclear astrophysics. The resonances, which persist down into the Gamow window, hinder our understanding of fusion rates in massive stars. In this chapter, we will review two aspects of $^{12}C+^{12}C$ clustering: the potential for observing transitions between cluster states, and the decay of cluster states into normal states (heavy-ion radiative capture).

2.4.1 Searching for Transitions Within $^{12}C + ^{12}C$ Cluster Bands

It is straightforward to access the cluster configuration in ^{8}Be as it is expected to already be the configuration of the ground state. In heavier, alpha-conjugate nuclei, this is much more difficult as the cluster states lie at a high excitation energy beyond the particle-breakup thresholds. Nevertheless, a number of attempts have been made to observe transitions within cluster bands, in particular, $^{12}C + ^{12}C$ configurations in ^{24}Mg. The observation of such transitions would indeed be the "smoking gun" in favour of the molecular hypothesis. Several calculations exist for transition strengths within the $^{12}C + ^{12}C$ cluster bands, for example those by Baye and Descouvemont within the GCM model [21]. Langanke and van Roosmalen [22] have also made such calculations and present predicted gamma widths for cluster states. A complication from the experimental perspective is that in reality the

cluster states appear somewhat fragmented and there is often not a unique state of a given spin/parity but rather a number of close-lying resonances. McGrath et al. [23] looked speculatively for gamma transitions between 14^+ and 12^+ "gross structure" $^{12}C + ^{12}C$ resonances. They did not search for the γ ray directly but instead looked for evidence of such a transition having taken place through detection of coincident heavy ions and measurement of the reaction Q-value. Haas et al. [24] made a more direct search for the in-band gamma ray in the $^{12}C + ^{12}C$ cluster band using the Château de Cristal, a large 4π array of BaF_2 scintillators. In particular, this study focussed on a possible γ-ray transition between 10^+ and 8^+ resonant states formed in the $^{12}C + ^{12}C$ reaction. The bombarding energy, $E_{lab} = 32.9$ MeV, was chosen to populate a known and isolated 10^+ resonance. The exotic branch of interest was searched for by looking for triple coincidences between γ rays and binary (e.g. $^4He + ^{20}Ne$,$^8Be + ^{16}O$ or $^{12}C + ^{12}C$) fragments. A handful of events were observed that fitted the necessary criteria but due to a high background, a clear and positive discrimination of the gamma branch was challenging. Nevertheless, a radiative partial width of $(1.2 \pm 0.4) \times 10^{-5}$ was deduced for the 10^+ resonance.

There is clearly scope to return to the search for in-band transitions. It might be better, for example, to attempt to locate transitions between lower spin members of the $^{12}C + ^{12}C$ cluster configuration where the phase space is more restricted. An improved measurement could be made with state-of-the-art detectors such as annular silicon strip detectors and with novel, high energy resolution scintillators like $LaBr_3$(Ce).

2.4.2 *Connecting Carbon-Carbon Resonances to Low-Lying States: Heavy-Ion Radiative Capture*

Heavy-ion radiative capture (HIRC) is an exotic and barely studied process but nevertheless has considerable application to the challenge of clustering in alpha-conjugate nuclei. An extensive review of this technique and of important work at Brookhaven National Laboratory on this topic in the 1980s is given by Sandorfi elsewhere [25] and so it is appropriate only to summarise it here before bringing it up-to-date.

The Brookhaven studies focussed on heavy-ion radiative capture in the $^{12}C + ^{12}C$ and $^{12}C + ^{16}O$ reactions. Sandorfi and Nathan employed a single large sodium iodide detector to detect high-energy capture gamma rays [26]. Such an approach is viable because the Q-value for radiative capture is large and positive for the reactions of interest and so the radiative capture events can be readily separated from other gamma rays associated with particle-emission channels, which completely dominate the total reaction cross-section, solely on the basis of their high energy. Sandorfi scanned the region between $E_{c.m.} = 5$ and 11 MeV for radiative capture resonances. The detection method used was sensitive to capture to the ground state, first, second and third (the latter unresolved) excited states (see Fig. 2.4). A series of resonances

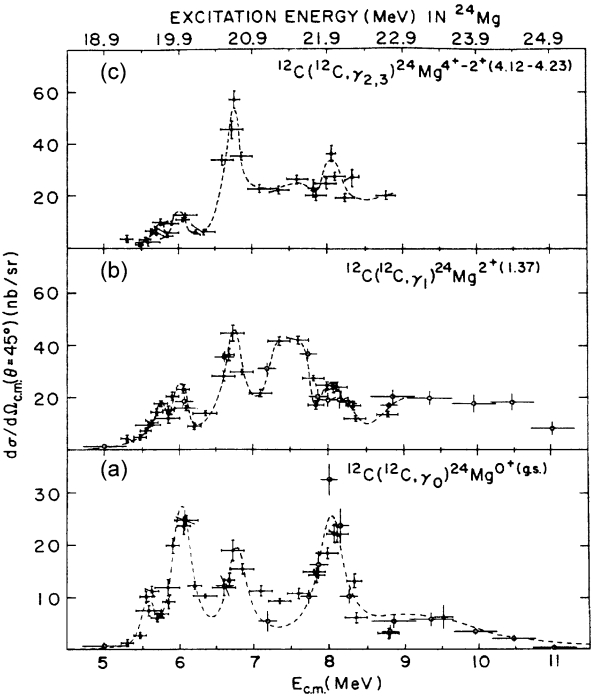

Fig. 2.4 Cross-sections for radiative capture to low-lying states in ^{24}Mg taken from [25]

were observed—some in individual channels and some clearly correlated between different channels. The observed resonances were typically 200–300 keV wide and corresponded to cross-sections of 10s of nanobarns per steradian.

By definition, the resonances observed must be low spin since the capture takes place directly to the ground state and first few excited states ($J = 2$ or 4). The resonances disappear towards the upper end of the energy range studied which either indicates that the cross-section begins to be distributed into other exit channels and/or the spin of the capture resonances is increasing and so they no longer directly feed the low-lying states in ^{24}Mg. The resonances were interpreted as a coupling to the giant quadrupole resonance strength in ^{24}Mg.

There are other reaction mechanisms which are in some sense the time inverse of the radiative capture process. The break-up of ^{24}Mg into two ^{12}C nuclei has been studied through electrofission around 30 years ago [27, 28]. There ought to be a relationship with the radiative capture data where excitation of the fissioning state proceeds through *E2* excitation. This comparison is complicated, however, by the potential to excite also through *E0*, *C0* and *C2* excitations. In addition, capture can proceed to excited states while electrofission is driven up from the ground state. Some structure is seen in the electrofission excitation function in a similar energy range to that seen in radiative capture, but a definitive interpretation of these results is not available [27, 28]. There would be value in repeating these measurements with state-of-the-art detectors.

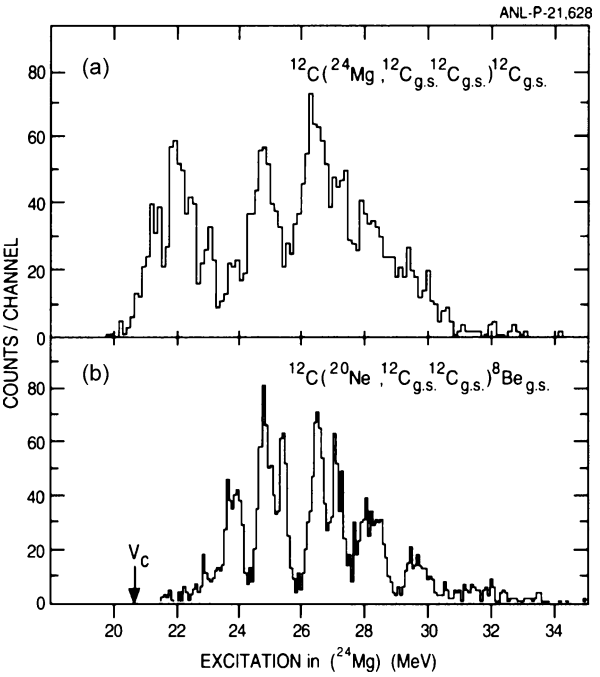

Fig. 2.5 Excitation energy spectra of ^{24}Mg in the reaction $^{12}C(^{24}Mg,^{12}C^{12}C)^{12}C$ at 170 MeV (*top*) and in the $^{12}C(^{20}Ne,^{12}C,^{12}C)^{8}Be$ reaction at 180 MeV [29]

The second mechanism related to the radiative capture mechanism is break-up. In such reactions, for example, ^{24}Mg is broken up into ^{12}C fragments through interaction with a ^{12}C target (see Fig. 2.5) [29–31]. This work was carried out around a decade following the initial radiative capture studies at Brookhaven. Qualitatively similar structure is seen in break-up as in the radiative capture but in a higher energy range, and the two sets of data overlap only over a very limited range. Again, the mechanism is roughly a time-inverse of radiative capture to the ground state. It is currently an open question as to how far these different reaction mechanisms explore different aspects of the underlying physics.

Returning to the HIRC mechanism, it is clear that the strong advantage of this approach is that it couples the resonances directly to excited states in ^{24}Mg. The strong limitation of the Brookhaven studies, however, was that they were restricted to a study of capture transitions to the ground state and the first few excited states, so what was observed might only be the "tip of the iceberg" in terms of the total capture cross-section. Moreover, the Brookhaven work could not search for transitions to highly-excited states in ^{24}Mg (see Fig. 2.6). An interesting speculation is whether there might be structural selectivity in the capture process so that enhanced transitions are seen to strongly-deformed (superdeformed) bands at high excitation energy. This is plausible for two reasons. Firstly, Collins et al. claimed to see preferential capture in the $^{12}C(^{16}O,\gamma)$ reaction to the excited prolate band rather than the oblate ground state band [32]. Secondly, there are long standing predictions of shape-isomeric/superdeformed (the nomenclature varies) bands with band-heads at

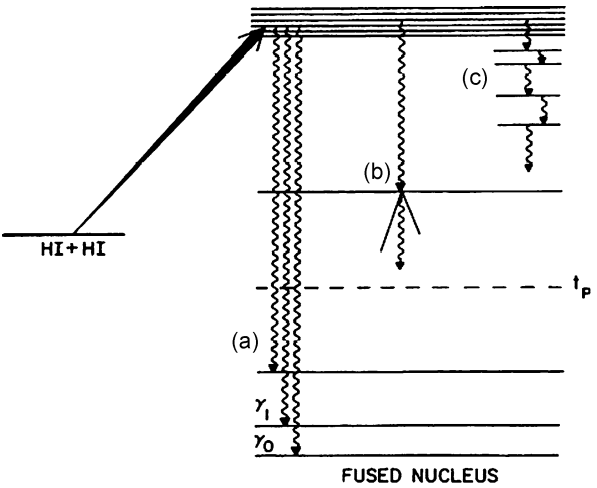

Fig. 2.6 The three possible modes of heavy ion radiative capture: (**a**) direct transitions to low-lying states (**b**) transitions to high-lying, potentially particle-unbound states (**c**) multi-step decay through yrast states (taken from [25])

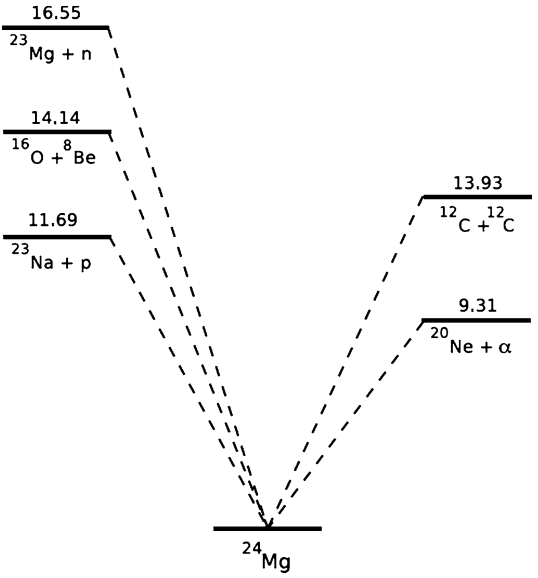

Fig. 2.7 The excitation energy for break-up of ^{24}Mg into different channels

around 10 MeV in ^{24}Mg and ^{28}Si (see the extensive discussion on candidates for the latter in the section below).

The principal challenge in the study of heavy-ion radiative capture is effectively identifying HIRC events and discriminating them from the overwhelming background due to particle-emission (see Fig. 2.7). This challenge is further complicated by the potential for target impurities, e.g. ^{13}C and ^{16}O in a ^{12}C target which can lead to confusion in the identification of true HIRC events. Two techniques are able to confront these challenges—the first is effectively sum-energy calorimetry, which is related to the original Brookhaven approach [25], while the second

is to use a recoil separator to rigorously identify HIRC residues. Both these approaches have been applied in the last ten years in renewed study of HIRC through a series of measurements at different laboratories in North America including Argonne National Laboratory, TRIUMF and Lawrence Berkeley National Laboratory.

2.4.3 Total Cross-Section Measurements

Jenkins *et al*. used the Fragment Mass Analyser (FMA) at Argonne National Laboratory to carry out an integrated cross-section measurement for the ^{12}C(^{12}C,γ) reaction at energies around $E_{c.m.} = 7.8$ MeV [33]. The cross-section was found to be around 3 μb which is a factor of three larger than the typical values seen in the earlier Brookhaven work [25, 26]. This coincides with the view that what was measured earlier was only a fraction of the total and that pathways through high-lying states must be important. A follow-up experiment was conducted using the Gammasphere array at Lawrence Berkeley National Laboratory. Gammasphere comprises 100 high-purity germanium detectors arranged in a spherical geometry [33]. Each detector (see Fig. 2.8) comprises a germanium crystal surrounded by a contiguous shield and suppressor plug made from Bismuth Germanate (BGO). The standard mode of operation for such a detector is for the BGO shield to act as a veto detector for gamma rays which scatter out of the germanium crystal. In this way, the peak-to-total can be dramatically improved. The design of Gammasphere, however, is optimised for detection of low energy (100–3000 keV) γ rays with high multiplicity. This is the kind of regime typified by a high-spin study of a deformed rare-earth nucleus where a long cascade of gamma rays results from the population of the nucleus of interest at a spin up to $50\hbar$. Unfortunately, HIRC studies have very different characteristics, namely a low multiplicity of gamma rays (including one single gamma ray) and typically high energy (2–20 MeV) gamma rays. The efficiency of Gammasphere for detecting gamma rays above 10 MeV in suppressed germanium detectors is essentially zero. These issues pose strong limitations on what can be achieved with Gammasphere in its conventional mode of operation. It is also possible, however, to operate in an add-back mode where the energy recorded in the BGO shield is added to that recorded in the germanium crystal, so that each element acts as effectively a composite detector module. The sum of such add-back energies recorded in the calorimeter as a whole can be used as a measure of the sum energy of the event. This technique was used in the Gammasphere experiment at Lawrence Berkeley National Laboratory [33], whereby a high-sum energy cut was imposed to separate the radiative capture channel from competing particle-evaporation channels (see Fig. 2.9).

Analysis of the Gammasphere data allowed the capture process to be explored in a limited fashion, and it was found that capture transitions to the $K = 2$ rotational band were prominent on-resonance, but appeared to be strongly suppressed off-resonance. The statistics available did not allow a detailed study of this effect.

Fig. 2.8 Schematic of a Gammasphere detector module

2.4.4 Strength Distribution Measurements Using DRAGON

While the FMA measurement showed that a significant part of the capture cross-section was missing, the low statistics of the Gammasphere experiment did not permit a detailed understanding of the decay process. Clearly, much higher efficiency was needed and this motivated a study by Jenkins et al. [34] of decay strength distributions in the ^{12}C(^{12}C,γ) reaction with the DRAGON recoil separator at TRIUMF. DRAGON [35] is specially constructed for nuclear astrophysics experiments, particularly (p,γ) reactions in inverse kinematics, e.g. ^{21}Na(p,γ) [36]. An array of close-packed BGO detectors surrounds the target position (normally a windowless gas target for nuclear astrophysics studies) which can be used to detect capture gamma rays (see Fig. 2.10). DRAGON comprises a two-stage recoil mass separator with a total length of 21 m. Separation of recoils from scattered beam is achieved using a combination of electric and magnetic dipoles. A single (optimal) charge state is selected in the first magnetic dipole. Energy dispersion in the electric dipole

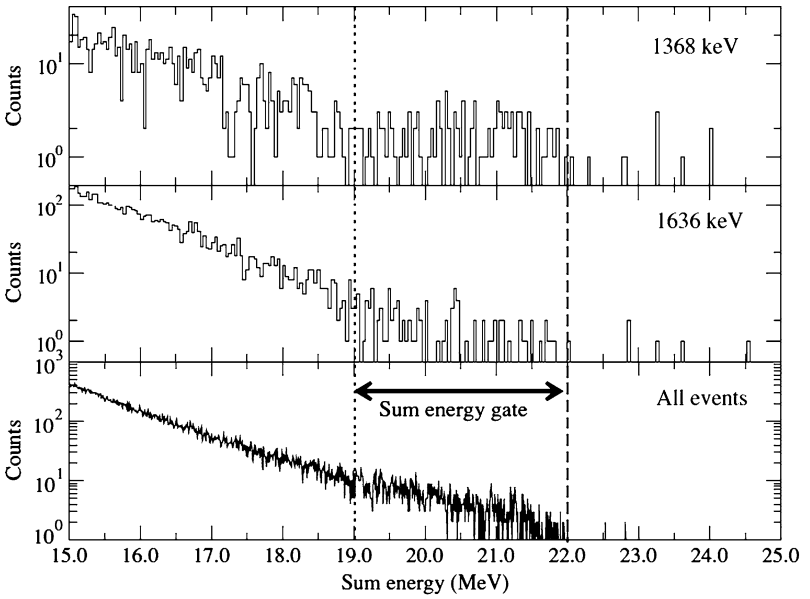

Fig. 2.9 Sum energy spectra in coincidence with 1368-keV transition in ^{24}Mg (*top*); 1636 keV transition in ^{23}Na (*middle*) and all events (*bottom*)

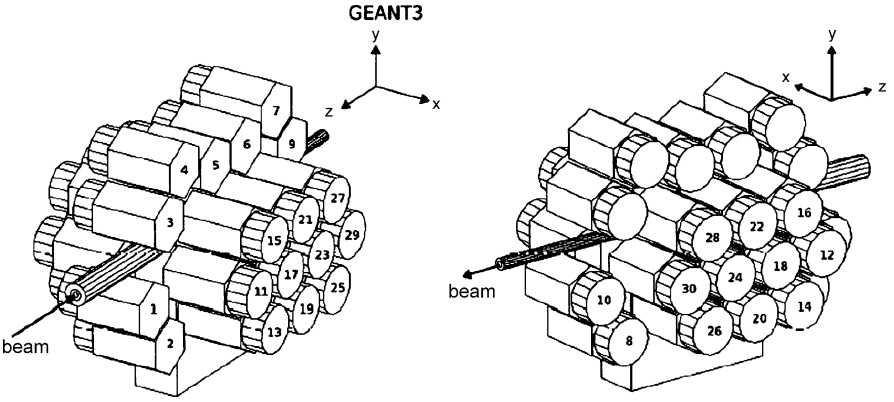

Fig. 2.10 Arrangement of BGO detectors around the DRAGON target position

separates the residues by mass. The second stage repeats this process, leading to an extremely high beam rejection ratio (10^{14}). Such a high rejection ratio is essential to DRAGON's intended application to studying proton capture reactions with short-lived radioactive species in inverse kinematics. Although not specifically designed for such an application, DRAGON is also an excellent tool for studies of heavy-ion radiative capture reactions. A disadvantage of the design, however, is that the angular acceptance of the device is limited due its intended application to (p, γ)

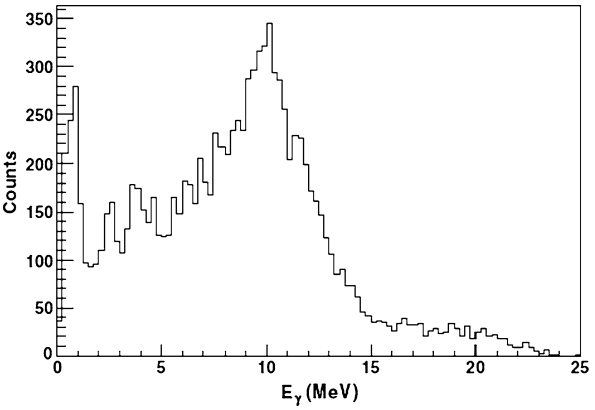

Fig. 2.11 Total projection of gamma rays in coincidence with recoils at $E_{cm} = 6.0$ MeV

reactions. The maximum recoil cone for ^{12}C(^{12}C,γ) at energies near the Coulomb barrier falls outside of this angular acceptance. In addition the layout of the BGO detectors around the target position is somewhat irregular and designed to maximise efficiency rather than symmetry. As a consequence of the design of DRAGON and the BGO array, it was necessary to carry out detailed GEANT3 simulations in order to understand the efficiency for different types of event. For the HIRC studies, the windowless gas target system was replaced with a solid target ladder.

Measurements of the ^{12}C(^{12}C,γ) reaction were made at a series of energies including the prominent capture resonances at $E_{cm} = 6.0$, 6.7, 7.5 and 8.0 MeV, as well as intermediate off-resonance energies. The radiative capture spectra obtained were compared to the results of a GEANT3 simulation to assist with the interpretation. This simulation incorporated decays to all known bound states via transitions with average transition strength taken from tabulated values.

The data at $E_{cm} = 6.0$, 6.7 MeV were relatively similar in that capture to the low-lying states was observed, consistent with the earlier Sandorfi work but the gamma-ray spectrum was dominated by a peak around 10 MeV (see Fig. 2.11). Such a feature could not have been seen in the earlier HIRC studies of Sandorfi et al. [27] as they only employed a single large sodium iodide detector.

Comparison with simulation suggests that the origin of the peak around 10 MeV is attributed to decay pathways via $T = 1$, 1^+ states in the region around 10 MeV in ^{24}Mg. These states are reached via strong isovector *M1* transitions. This previously unseen decay mechanism is analogous to Gamow-Teller beta decay (see Fig. 2.12). In order to populate such states in the decay, the capture resonance must have spin/parity of 0^+ or 2^+; the comparison with simulation gives strong preference to the latter. Comparing the capture spectra with simulations for two further resonances at $E_{cm} = 7.5$ and 8.0 MeV suggests $J = 4^+$ assignments (or a mixture of 2^+ and 4^+ for $E_{cm} = 8.0$ MeV). It is interesting to cross-reference this new information with break-up data where $J = 4$ resonances are seen at $E_{cm} = 7.3$ and 7.7 MeV [31].

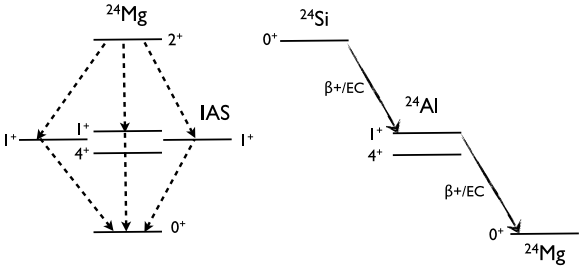

Fig. 2.12 Comparison between radiative capture via IAS $T = 1$ states (*left*) and Gamow-Teller beta decay (*right*)

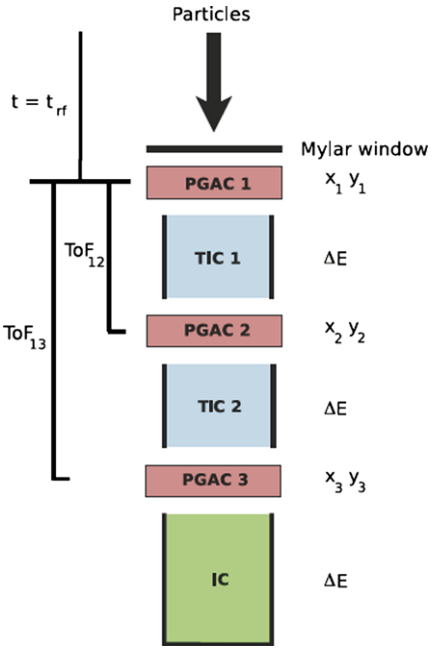

Fig. 2.13 Multi PGAC-ion chamber system

2.4.5 Gammasphere and FMA

The lessons learned from previous techniques applied to the study of the $^{12}C(^{12}C,\gamma)$ reaction suggested that the key features needed in any future study would be robust channel selection with no bias towards any class of residues, allied to a high energy resolution for detection of capture gamma rays. In 2007, an experiment was carried out to obtain high statistics for the capture process with high energy resolution by focussing on one specific capture resonance in the $^{12}C(^{12}C,\gamma)$ reaction at $E_{c.m.} =$ 8.0 MeV [37]. The Gammasphere array was used to detect the capture gamma rays, while the FMA was used to separate residues by A/q. A robust selection of the capture channel was achieved using a multi-step ion chamber/PGAC system [38] illustrated in Fig. 2.13. By producing a 2D spectrum of the energy loss (ΔE) versus

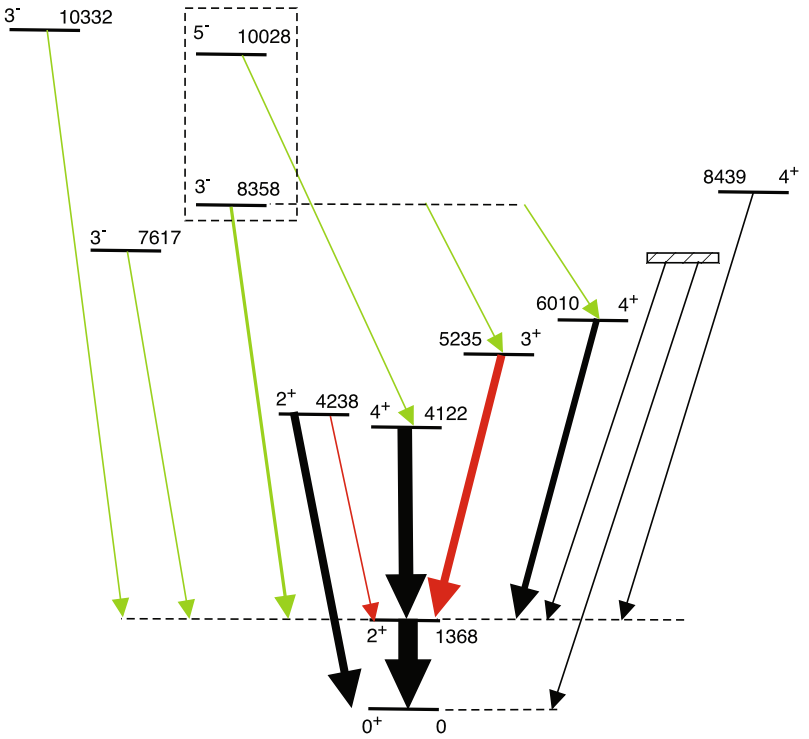

Fig. 2.14 Levels populated in ^{24}Mg following radiative capture. The *green* transitions are E1, *red* transitions are M1/E2 and *black* transitions are E2

the time of flight (ToF) through each of the two transmission ionisation chambers (TICs) it was possible to unambiguously identify ^{24}Mg despite the overwhelming dominance of the particle evaporation channels [37].

The residue selection afforded a reduction in the intensity of contaminant channels by five orders of magnitude. This allowed the decay branching of the capture resonance to be examined in detail (see Fig. 2.14). In general, the population of positive parity states appeared to demonstrate a statistical feeding expected for the decay of the resonance by *E2* transitions. The observed feeding strongly favoured a $J^\pi = 4^+$ assignment to the capture resonance. There are two aspects in support of this. Firstly, states between 2^+ and 5^- are fed, but no lower spin states. This strongly disfavours a spin/parity assignment of 0^+ or 2^+ to the capture resonance. Moreover, in the earlier studies with DRAGON discussed above, capture resonances with $J^\pi = 0^+$ and 2^+ had very strong decays to 1^+, $T = 1$ states via isovector *M1* transitions. These were not observed in the Gammasphere study.

The surprising feature of the data was the strong population of the 3^- state at 8358 keV and 5^- level at 10028 keV, amounting to a total of $\sim$18 % of the feeding intensity (see Fig. 2.15). These states were identified as members of a

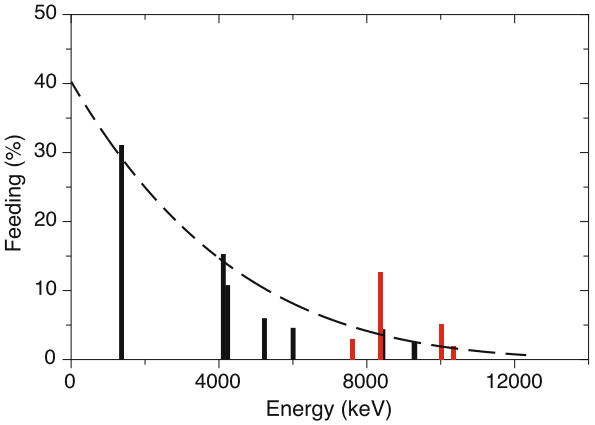

Fig. 2.15 Feeding pattern for population of states following radiative capture for the ^{12}C(^{12}C,γ) reaction at $E_{c.m.} = 8.0$ MeV. Cascade feeding has been removed. The population of negative parity states is shown in red

$K^\pi = 0^-$ band by Branford et al. on the basis of the strong *E2* transition connecting the two states [39]. It is notable that the feeding of the 3^- and 5^- states in the $K^\pi = 0^-$ band is enhanced 3–5 times relative to the other 3^- states observed. An open question is whether this enhancement is structural in origin. Kato and Bando [40] find in their cluster calculations that the $K^\pi = 0^-$ band corresponds to the parity doublet of the ground state band. As discussed by Butler and Nazarewicz in their review of octupole phenomena in nuclei [41], there are similar predictions of low-lying $K^\pi = 0^-$ bands in many light alpha-conjugate nuclei. Branford et al. note that while the candidate $K^\pi = 3^-$ band has a similar moment-of-inertia to the ground-state band, the moment-of-inertia of their candidate $K^\pi = 0^-$ band is more than double that of the ground-state band. This would imply that the $K^\pi = 0^-$ band is associated with a large deformation.

In their transfer-reaction study, Tribble et al. showed that the lowest 3^- state in ^{24}Mg had a structure mostly related to a hole in the $1p$ shell, while the second 3^- state appeared to be better explained as a particle-hole excitation into the *fp* shell [42]. This observation seems to be borne out by $1\hbar\omega$ PSDPF shell model calculations which indicate that the lowest 3^- state is clearly associated with a $1p$ hole, while the first 5^- state is clearly associated with a particle in the *fp* shell. The second 3^- state is a mixture of these two configurations. Naturally, the model space is somewhat restricted and, in a deformed nucleus, the $1p$-$1h$ configurations might also be expected to have significant $3p$-$3h$ components. It is interesting that in a two-centre shell model study of the $^{12}\mathrm{C} + {}^{12}\mathrm{C}$ system, Chandra and Mosel [43] pointed to a major component for configuration for the molecular resonances of $4p$-$4h$. Again, such configurations would be expected to have $2p$-$2h$ components as well. Favoured decay between these particle-hole excitations might, therefore, be anticipated in comparison to decay to the configurations based on a $1p$ shell hole. This could explain the favoured decay to the second 3^- and first 5^- states.

2.4.6 Studies of the $^{12}C(^{16}O,\gamma)$ Reaction

The $^{12}C(^{16}O,\gamma)$ reaction was also investigated at Brookhaven National Laboratory in the 1980s [32]. A more sophisticated set-up was used compared to the $^{12}C(^{12}C,\gamma)$ studies, in that a Wien filter and ionisation chamber were coupled to a single sodium iodide detector. This allowed capture residues to be more rigorously identified but the single detector involved still posed a limitation in that only gamma-ray singles could be studied and not coincidence data. The $^{12}C(^{16}O,\gamma)$ data were qualitatively different to the earlier $^{12}C(^{12}C,\gamma)$ study in that there appeared to be preferred feeding of the 0_3^+ state which is the bandhead of the prolate (normal-deformed) band in ^{28}Si [32]. This preferential feeding was attributed to the greater structural overlap between the entry resonance and the prolate band, as opposed to the oblate, ground-state band.

The $^{12}C(^{16}O,\gamma)$ reaction has also been reinvestigated in the last few years using the DRAGON recoil separator and its associated BGO array. In certain respects, the situation is less straightforward since non-identical bosons are involved and so negative-parity resonances are also possible, effectively doubling the number of potential resonances. In addition, E1 transitions are much more important.

Three energies were investigated using DRAGON [44, 45], corresponding to $E_{cm} = 8.5$, 8.8 and 9.0 MeV coinciding with the region explored earlier by Collins et al. [32]. The data obtained were analysed in a similar manner to the $^{12}C(^{12}C,\gamma)$ study, using a Monte Carlo simulation of the full electromagnetic elements of the DRAGON separator and the BGO array. This is important as the acceptance into DRAGON is not 100 % for this class of reaction. The $E_{cm} = 9.0$ MeV resonance appears to have a clear unique spin of 6^+, while the other resonances are best fit with a mixture of contributions from spins of 5^- and 6^+.

The key result of the recent $^{12}C(^{16}O,\gamma)$ study was to show that what was earlier interpreted as feeding of the excited prolate bandhead was incorrect, and that the feeding in fact proceeds to a close-lying 3^- state which is the bandhead of a $K^\pi = 3^-$ band. The change in the interpretation of the data is a feature of the availability of γ-γ coincidence data, which were not available in the original studies in the 1980s.

2.5 Superdeformed Bands and Clustering

The term "superdeformed" is most generally associated with the discovery of bands in rare-earth nuclei like ^{152}Dy [46]. This term has also been applied, however, to rotational bands in the light, alpha-conjugate nuclei, ^{36}Ar [47] and ^{40}Ca [48], which were identified around ten years ago, in γ-ray spectroscopy studies. Figure 2.16 shows the level scheme for ^{40}Ca, where there is shape coexistence between the spherical ground state, a prolate deformed band with a band-head at 3.352 MeV and the superdeformed (SD) band with its band-head at 5.213 MeV. It is instructive to compare the gamma-ray spectroscopy work with earlier transfer reaction studies as the latter can point to the clustering structure of the states. Middleton et al. [49]

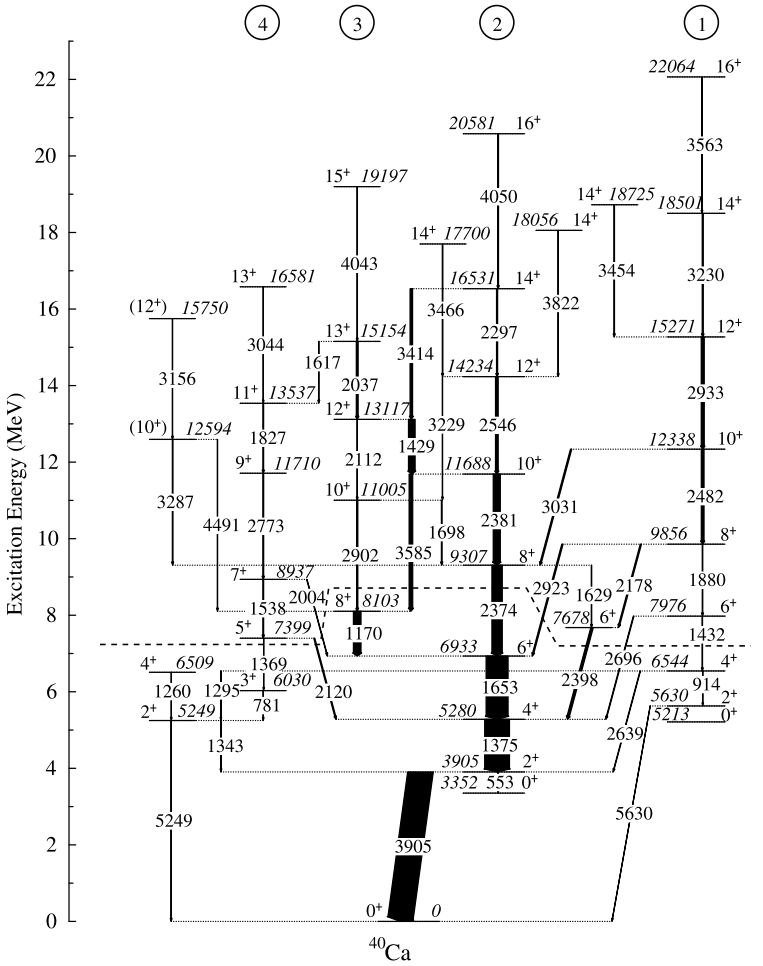

Fig. 2.16 Level scheme for ^{40}Ca. The prolate ($4p$-$4h$) is labelled as band 2. The superdeformed ($8p$-$8h$) band is labelled as band 1 (taken from [48])

studied the ^{32}S(^{12}C,α)^{40}Ca reaction, where the 0^+ state at 3.352 MeV attributed to the $4p$-$4h$ configuration is excited ten times more strongly than the $0p$-$0h$ configuration, and the $8p$-$8h$ is excited 1.5 times more strongly than the $4p$-$4h$ (see Fig. 2.17). Indeed, the state most strongly excited in this reaction is at 7.98 MeV in ^{40}Ca, which has latterly been shown to be the 6^+ state in the superdeformed band in ^{40}Ca based on the $8p$-$8h$ configuration [48].

The superdeformed bands in ^{36}Ar and ^{40}Ca are of particular interest, since a complementary description can be found both in terms of particle-hole excitations in the shell model, and from cluster model calculations such as antisymmetrized molecular dynamics (AMD) e.g. [50]. This raises the question of whether clustering is the correct description or whether cluster models simply agree with the appear-

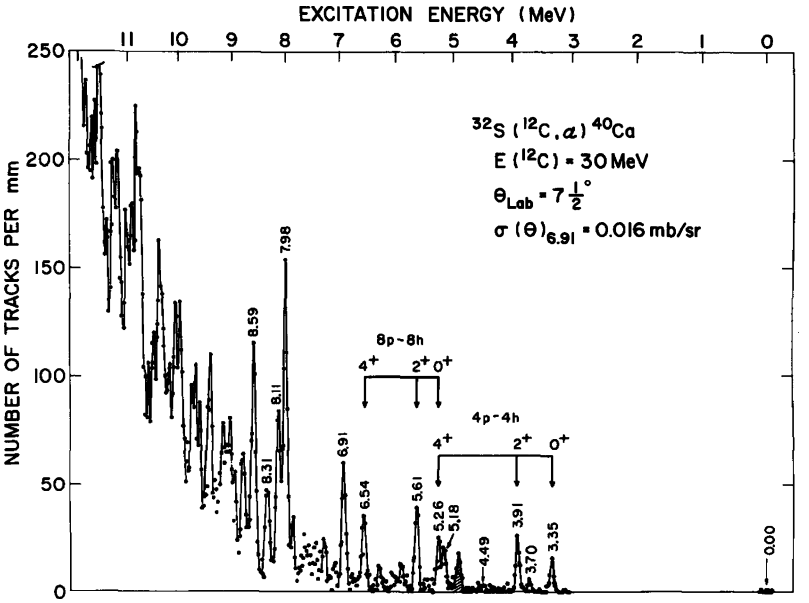

Fig. 2.17 Particle spectrum taken from [49]

ances. One way to test this is to observe the evolution from clustered to deformed regimes. For this, it would be highly desirable to locate superdeformed bands in lighter, alpha-conjugate nuclei such as ^{32}S and ^{28}Si for which long-standing theoretical predictions of superdeformed configurations exist and which remain a hot topic for theoretical study e.g. ^{32}S [51]. From the experimental perspective, such an extension is very challenging as the superdeformed bands in ^{28}Si and ^{32}S are predicted to lie at much higher excitation energy than those in ^{36}Ar and ^{40}Ca. This leads to two consequences: Firstly, that phase space favours high energy out-of-band transitions compared to low energy in-band transitions despite the strong collective character of the latter. Secondly, the bandhead lies on or above the particle-decay thresholds meaning that there is competition with particle emission.

Recently, Taniguchi et al. [52] have made an extensive study of collective structures in ^{28}Si using the AMD model. They explored clustering degrees of freedom of the type: $^{24}\mathrm{Mg} + \alpha$ and $^{12}\mathrm{C} + {}^{16}\mathrm{O}$. These studies reveal a rich diversity of rotational behaviour (see Fig. 2.18). There is shape coexistence between the oblate ground state band and a prolate (ND) band. An SD band is identified in the calculations with a strong $^{24}\mathrm{Mg} + \alpha$ configuration as well as some component of $^{12}\mathrm{C} + {}^{16}\mathrm{O}$.

The AMD calculations show good correspondence with the known band structure of ^{28}Si, which comprises an oblate ground state band, co-existing with a prolate rotational band. It is more difficult to find states forming likely candidates for the SD band. In their recent paper, Taniguchi et al. [52] compare their predictions for the SD band in ^{28}Si with the properties of a so-called "excited prolate" band identified in the early 1980s by Kubono et al. [53] using the $^{12}\mathrm{C}(^{20}\mathrm{Ne},\alpha)^{28}\mathrm{Si}$ reac-

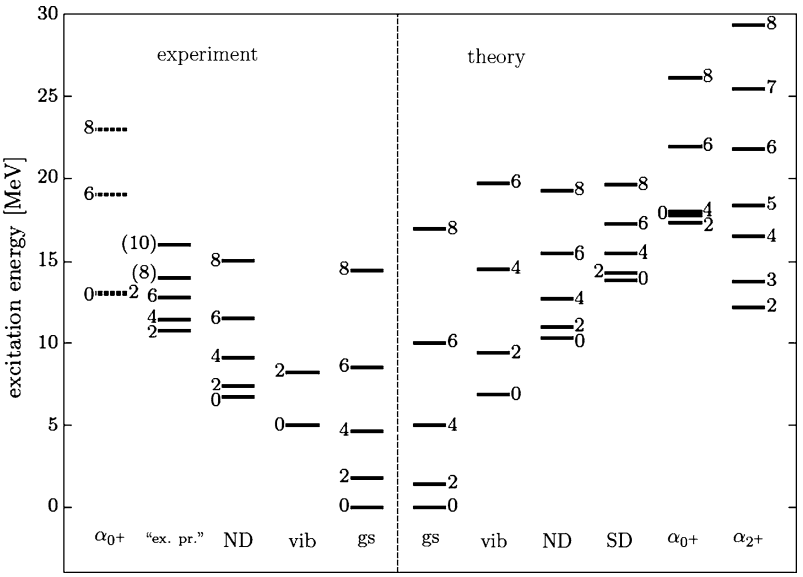

Fig. 2.18 Comparison of known experimental bands in ^{28}Si with predictions of the AMD model (taken from [52])

tion. The experimental assignment of this "excited prolate" band rests on peaks in a charged particle spectrum, many of which do not have well-established spin/parity. These states, however, do not form a smooth sequence characteristic of a rotational band even making plausible allowance for mixing (see Fig. 2.19), and the suggested moments of inertia are rather higher than the calculated values. Moreover, γ-ray transitions between these states are not observed, and, as a consequence, transition strengths are unknown. Without the observation of in-band transitions, assigning candidate rotational bands is difficult and potentially ambiguous, although such an approach has been a common procedure in the past for "cluster" bands in light nuclei.

The striking feature of the AMD calculations, however, is the dominant $^{24}\mathrm{Mg}+\alpha$ component and this poses the question as to whether the $^{24}\mathrm{Mg}(\alpha,\gamma)$ radiative capture reaction might prove to be a favoured reaction mechanism for selectively populating SD states in ^{28}Si. A review of the literature on this reaction suggests some possible candidate SD states, in particular, the 12.86 MeV state which has decay branches to a number of states including a 4^+ state at 10.945 MeV, via a 1.921 MeV transition; the associated B(E2) value exceeds 25 Wu [55–57]. Comparison with the USD shell model leads to the conclusion that the respective 6^+ and 4^+ states as well as a 2^+ state at 9796 keV are not consistent with expected shell model states but are more likely to be intruder states. They suggest, accordingly, that the states they have identified form a candidate $K^\pi = 0^+$ intruder band. If this set of states did form a rotational band then the kinematic moment of inertia would be $6\hbar^2$/MeV, in good conformity to that predicted by the AMD calculation (see Fig. 2.19).

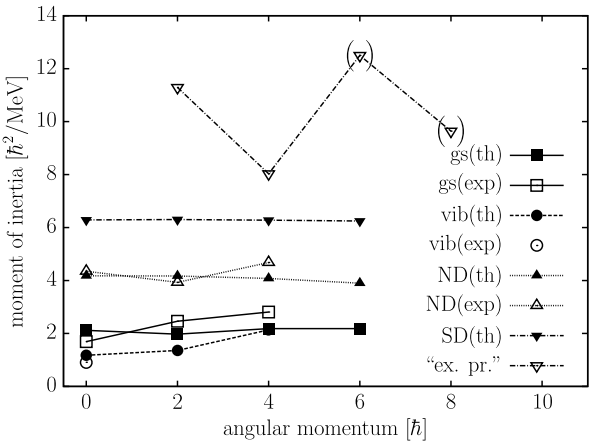

Fig. 2.19 Calculated and experimental moments-of-inertia for rotational bands in ^{28}Si taken from [52]

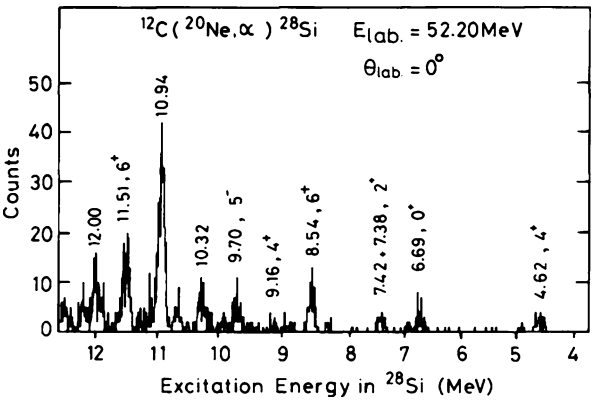

Fig. 2.20 Particle spectrum from the ^{12}C(^{20}Ne,α)^{28}Si reaction taken from [53]

The unusual character of the 10.94 MeV and 12.86 MeV states becomes clear when cross-referenced with other work such as the ^{12}C(^{20}Ne,α)^{28}Si reaction studied by Kubono et al. [53]. In this reaction, the 10.94 MeV state is the most strongly populated state below 12 MeV (see Fig. 2.20). This 4^+ state is populated with more than ten times the cross-section of the 4^+ states in the prolate and oblate ground state bands. The reaction mechanism is likely to favourably populate multi particle-hole states or in other words, those with substantial alpha clustering component.

Analysis of the ^{12}C(^{20}Ne,α)^{28}Si reaction provides a strong assignment of 6^+ to a 12.8 MeV state [53]. This state is also shown to have a direct proton branch to the $5/2^+$ ground state of ^{27}Al [53] which implies $L = 4$ and so there must be an associated $g_{9/2}$ component, corresponding to $S = 0.3$ [54]. This result is reinforced by a parallel ^{24}Mg(α, t) study by Kubono et al. [53, 54] which also indicated a sizeable $g_{9/2}$ component to the 12.82 MeV state. This is an unusually large component possibly reflecting a strong associated deformation. A consistent picture emerges, therefore, where the candidate intruder states discussed by Brenneisen et al. appear with unusual selectivity in the ^{12}C(^{20}Ne,α)^{28}Si reaction, and with the suggestion of

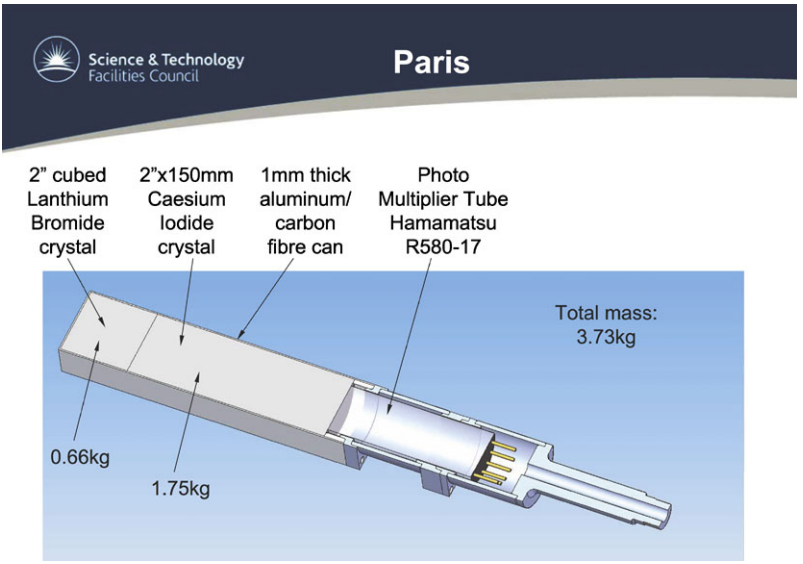

Fig. 2.21 PARIS phoswich design

very strong deformation, in the case of the 12.86 MeV state. Further work in this area is clearly warranted.

In the future, it would be of great interest to extend the knowledge of superdeformed bands to ^{24}Mg and ^{32}S. Given the synergies between transfer reactions and γ-ray spectroscopy discussed for the extant cases, it might be interesting to consider a particle-gamma study, where an alpha-particle transfer reaction is chosen to selectively populate the states of interest, and gamma-ray branches measured to confirm the band structure and extract B(E2) strengths.

2.6 Future Prospects and New Detector Materials

In all of the examples discussed above, gamma-ray spectroscopy studies related to clustering are restricted by the desire to achieve both high energy resolution and high efficiency. High energy resolution can be achieved with Compton-suppressed germanium detectors but at the expense of efficiency. Scintillator detectors provide much higher efficiency but at the expense of relatively poor energy resolution. Novel scintillator materials such as lanthanum bromide and cerium bromide are now becoming available which promise energy resolutions of around 3 %. They also have very fast time response which can be used to reject neutrons. The difficulty at the time of writing, however, is the high cost of such next generation detectors relative to conventional materials.

The PARIS collaboration (http://paris.ifj.edu.pl) intends to build a 4π calorimeter using novel scintillators. In particular, they are investigating using phoswich de-

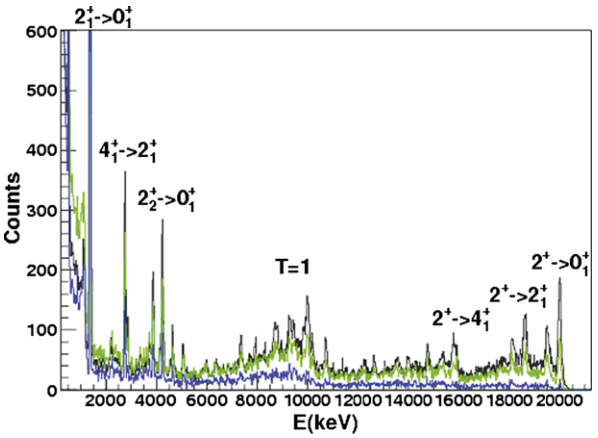

Fig. 2.22 Simulation of the performance of PARIS for the study of the $^{12}C(^{12}C,\gamma)$ reaction

tectors where a 2″ cubic crystal of $LaBr_3(Ce)$ is backed by a longer crystal of a conventional scintillator like sodium iodide (see Fig. 2.21). The advantage of such an arrangement is that it obtains most of the benefit of the novel material but at a reduced cost.

Use of novel scintillators in the future could lead to a step change in what can be achieved in cluster studies using gamma-ray spectroscopy. For example, Fig. 2.22 shows the results of a simulated study of the $^{12}C(^{12}C,\gamma)$ reaction using the PARIS calorimeter. Feeding of individual high-lying states is now readily resolvable. A definitive study of the heavy-ion radiative capture reactions is therefore, perhaps best achieved with a 4π PARIS. Channel selection would be achieved using calorimetry. Aside from HIRC studies, most of the types of study discussed above would profit from the use of scintillators with high energy resolution.

Acknowledgements I would like to acknowledge valuable discussions with Y. Kanada-En'yo and Y. Taniguchi. Sandrine Courtin and Florent Haas should be acknowledged for their careful reading of this manuscript.

References

1. E. Almqvist et al., Phys. Rev. Lett. **4**, 515 (1960)
2. D.A. Bromley, J.A. Kuehner, E. Almqvist, Phys. Rev. Lett. **4**, 365 (1960)
3. M. Freer, Rep. Prog. Phys. **70**, 2149 (2007)
4. R.R. Betts, A.H. Wuosmaa, Rep. Prog. Phys. **60**, 819 (1996)
5. J.L. Wood et al., Nucl. Phys. A **651**, 323 (1999)
6. E. Farnea et al., Nucl. Instrum. Methods A **621**, 331 (2010)
7. R. Guardiola et al., Nucl. Phys. A **679**, 393 (2001)
8. Y. Yamamoto, T. Togashi, K. Kato, Prog. Theor. Phys. **124**, 315 (2010)
9. R.B. Wiringa, S.C. Pieper, J. Carlson, V.R. Pandharipande, Phys. Rev. C **62**, 014001 (2000)
10. K. Langanke, C. Rolfs, Phys. Rev. C **33**, 790 (1986)
11. K. Langanke, C. Rolfs, Z. Phys. A **324**, 307 (1986)
12. V.M. Datar, S. Kumar, D.R. Chakrabarty, V. Nanal, E.T. Mirgule, A. Mitra, H.H. Oza, Phys. Rev. Lett. **94**, 122502 (2005)

13. F. Hoyle, Astrophys. J. Suppl. Ser. **1**, 121 (1954)
14. C.W. Cook et al., Phys. Rev. **107**, 508 (1957)
15. E. Epelbaum, H. Krebs, D. Lee, U. Meissner, Phys. Rev. Lett. **106**, 192501 (2011)
16. M. Freer et al., Phys. Rev. C **80**, 041303 (2009)
17. B. Buck, C.B. Dover, J.P. Vary, Phys. Rev. C **11**, 1803 (1975)
18. M. Chernykh et al., Phys. Rev. Lett. **105**, 022501 (2010)
19. T. Yamada et al., J. Phys. Conf. Ser. **111**, 012008 (2008)
20. E. Vogt, H. McManus, Phys. Rev. Lett. **4**, 518 (1960)
21. D. Baye, P. Descouvemont, Nucl. Phys. A **419**, 397 (1984)
22. K. Langanke, O.S. van Roosmalen, Phys. Rev. C **29**, 1358 (1984)
23. R.L. McGrath, D. Abriola, J. Karp, T. Renner, S.Y. Zhu, Phys. Rev. C **24**, 2374 (1981)
24. F. Haas et al., Nuovo Cimento A **110**, 989 (1997)
25. A.M. Sandorfi, in *Treatise on Heavy Ion Science*, ed. by D.A. Bromley (Plenum, New York, 1985). Vol. 2, Sect. III and references therein
26. A.M. Nathan, A.M. Sandorfi, T.J. Bowles, Phys. Rev. C **24**, 932 (1981)
27. A.M. Sandorfi, L.R. Kilius, H.W. Lee, A.E. Litherland, Phys. Rev. Lett. **40**, 1248 (1978)
28. A.M. Sandorfi, J.R. Calarco, R.E. Rand, H.A. Schwettman, Phys. Rev. Lett. **45**, 1615 (1980)
29. B.R. Fulton et al., Phys. Lett. B **267**, 325 (1991)
30. B.R. Fulton et al., J. Phys. G **20**, 151 (1994)
31. N. Curtis et al., Phys. Rev. C **51**, 1554 (1995)
32. M.T. Collins, A.M. Sandorfi, D.H. Hoffmann, M.K. Salomaa, Phys. Rev. Lett. **49**, 1553 (1982)
33. D.G. Jenkins et al., Phys. Rev. C **71**, 041301 (2005)
34. D.G. Jenkins et al., Phys. Rev. C **76**, 044310 (2007)
35. D.A. Hutcheon et al., Nucl. Instrum. Methods Phys. Res. A **498**, 190 (2003)
36. S. Bishop et al., Phys. Rev. Lett. **90**, 162501 (2003)
37. P. Marley et al., Phys. Rev. C **84**, 044332 (2011)
38. C.L. Jiang et al., Nucl. Instrum. Methods A **554**, 500 (2005)
39. D. Branford, N. Gardner, I.F. Wright, Phys. Lett. B **36**, 456 (1971)
40. K. Kato, H. Bando, Prog. Theor. Phys. **62**, 644 (1979)
41. P.A. Butler, W. Nazarewicz, Rev. Mod. Phys. **68**, 349 (1996)
42. R.E. Tribble, G.T. Garvey, J.R. Comfort, Phys. Lett. B **44**, 366 (1973)
43. H. Chandra, U. Mosel, Nucl. Phys. A **298**, 151 (1978)
44. S. Courtin et al., Acta Phys. Pol. B **42**, 757 (2011)
45. D. Lebhertz et al., AIP Conf. Proc. **1165**, 331 (2009)
46. P.J. Nolan, P.J. Twin, Annu. Rev. Nucl. Part. Sci. **38**, 533 (1988)
47. C.E. Svensson et al., Phys. Rev. Lett. **85**, 2693 (2000)
48. E. Ideguchi et al., Phys. Rev. Lett. **87**, 222501 (2001)
49. R. Middleton, J.D. Garrett, H.T. Fortune, Phys. Lett. B **39**, 339 (1972)
50. Y. Taniguchi, M. Kimura, Y. Kanada-En'yo, H. Horiuchi, Phys. Rev. C **76**, 044317 (2007)
51. M. Kimura, H. Horiuchi, Phys. Rev. C **69**, 051304 (2004)
52. Y. Taniguchi, Y. Kanada-En'yo, M. Kimura, Phys. Rev. C **80**, 044316 (2009)
53. S. Kubono et al., Nucl. Phys. A **457**, 461 (1986)
54. S. Kubono et al., Phys. Rev. C **33**, 1524 (1986)
55. J. Brenneisen et al., Z. Phys. A **352**, 149 (1995)
56. J. Brenneisen et al., Z. Phys. A **352**, 279 (1995)
57. J. Brenneisen et al., Z. Phys. A **352**, 403 (1995)

http://www.springer.com/978-3-319-01076-2

Clusters in Nuclei, Volume 3
Beck, C. (Ed.)
2014, XIV, 246 p. 167 illus., 92 illus. in color., Softcover
ISBN: 978-3-319-01076-2